Dynamics and structures of segregation in a dense, vibrating granular bed

Jin Sun, Francine Battaglia, and Shankar Subramaniam*
Department of Mechanical Engineering, Iowa State University, Ames, Iowa 50011, USA
(Received 2 August 2006; published 18 December 2006)

We study the rise dynamics of a large particle in a granular bed under vertical vibration using molecular dynamics simulations. Systematic variation of the particle properties and external wall friction in the simulations shows that the large particle rising is very sensitive to external wall friction. The dynamical response of the granular bed with wall friction is shown to include an expansion stage and a compression stage within one cycle. With wall friction, large-scale force networks bearing larger-than-average forces are found in the compression stage. However, without wall friction, large strong force networks do not exist. The distribution of normal contact forces in the force networks is found to have an exponential tail similar to those in packing experiments. Numerical estimation of the two-point spatial correlation of normal contact force reveals predominantly short-range force correlation persisting over only 2–3 particle diameters. The structural properties of the force network are analyzed using a graph-theoretic approach, which is a modification of a minimum spanning tree (MST) constructed on the particles in physical space. The modified MST algorithm, which identifies local structures such as nearest neighbors, asymptotically recovers all particle contacts, the force distribution, and spatial force correlation of the force network. This indicates that although wall friction strongly affects the rising dynamics of the Brazil nut over the device scale (tens of particle diameters) through the force network, it does so through local short-range interactions. Thus this study affirms the basis for local constitutive models in continuum descriptions of segregation.

DOI: 10.1103/PhysRevE.74.061307 PACS number(s): 45.70.Mg

I. INTRODUCTION

Segregation in granular media occurs both in nature and in industrial processes. Therefore, a fundamental understanding of the dynamics and mechanisms of segregation is of practical importance. A canonical problem in granular segregation is the rise or fall of a large particle in a bed of small particles as a consequence of vibration applied to the granular bed. This phenomenon was first named the "Brazil nut problem" (BNP)[1] by Rosato *et al.* [2], who used a Monte Carlo method to study this problem. Since then there have been extensive experimental studies, theoretical investigations, and computer simulations of the BNP. Simulation of the BNP is acknowledged as a benchmark of granular segregation.

Granular segregation observed in the BNP is dependent on particle properties, flow conditions and external boundary conditions, and is not explained by a single mechanism. While many mechanisms have been proposed from different perspectives to explain the BNP phenomenon, no unified theory has yet emerged and our understanding is still incomplete. This is in part because the mechanisms do not solely manifest themselves in clearly demarcated regimes, but rather they appear to coexist across different regimes. The problem is further complicated by the interaction between different time and length scales, which is affected by the bed vibration parameters, namely, the amplitude and frequency [3].

The vibration parameters can be characterized by the dimensionless amplitude A_0/d_0, where A_0 is the vibration amplitude and d_0 is the particle diameter, and the dimensionless frequency $\omega_0\sqrt{d_0/g}$. When characterizing the dynamics of the BNP, these appear in combination as a dimensionless acceleration $\Gamma=A_0\omega_0^2/g$, which characterizes the acceleration due to external forced vibration relative to gravity.

Some segregation mechanisms may be classified into two categories according to the acceleration and frequency in the system [4]. For $\Gamma>1$ and low frequencies, convection, and inertia are proposed as segregation mechanisms. Convection, where particles descend along vertical (frictional) walls and ascend at the center, is proposed as the dominant mechanism [5] when ρ_r, the relative density of the large particle to small particles, is less than a critical value ρ_{rc} ($\rho_{rc}\approx 0.57$ from experiments in Ref. [6]). On the other hand, inertia dominates when $\rho_r>\rho_{rc}$. The inertia effect is believed to dominate segregation in the granular system studied in this paper, where $\Gamma=3.39$, $\omega_0\sqrt{d_0/g}=0.67$, and $\rho_r=7.09$ (calculated from parameters in Table I).

For $\Gamma>1$ with small amplitudes and high frequencies, where the granulate is fluidized without convection, a "buoyancy force" analogous to fluid buoyancy has been proposed to predict the Brazil nut effect [7,8]. Other mechanisms from topological considerations have also been proposed, such as arching [9] and "void filling" beneath large particles [3]. In addition to these mechanisms, air-driven segregation has also been found to be important in the case of very fine particles [10–12]. Despite the variety of mechanisms proposed, many important details of the microscopic dynamics driving the segregation remain unknown. For instance, while the existence of force chains in three-dimensional vibrating granular systems and its role in the segregation have been hypothesized [13], the sensitivity of the force chain formation to external boundary conditions is still unclear.

In this paper, we investigate the segregation dynamics of the BNP using molecular dynamics (MD) simulations, which

*Corresponding author. Electronic address: shankar@iastate.edu

TABLE I. Basic computational parameters settings.

	Small particle	Large particle
Number of particles	7600[a]	1
Particle diameter	d_0	3.16 (d_0)
Particle density	1.91 (m_0/d_0^3)	13.54 (m_0/d_0^3)
Particle normal stiffness coefficient k_n	$2\times10^5(k_0)$	
Particle tangential stiffness coefficient k_t	$\frac{2}{7}k_n$	
Particle normal damping coefficient γ_n	$40(1/t_0)$	
Particle tangential damping coefficient γ_t	$0(1/t_0)$	
Particle friction coefficient μ	0.5	
Background damping coefficient b	0 for most cases ($m_0\sqrt{g/d_0}$)[b]	
Particle restitution coefficient	0.9	0.86
Wall normal stiffness coefficient	$2\times10^5(k_0)$	
Wall tangential stiffness coefficient	$\frac{2}{7}k_n$	
Wall normal damping coefficient	$40(1/t_0)$	
Wall tangential damping coefficient	$20(1/t_0)$	
Wall friction coefficient μ_{wall}	0.5	
Vibration frequency	$0.107(1/t_0)$	
Vibration amplitude A_0	$7.5(d_0)$	
Time step	$2\times10^{-4}(t_0)$	

[a]In some cases 6000 small particles were used to test different bed heights. It is shown that this difference does not affect the rising dynamics

[b]Expect the cases with background damping or air damping

allow us to systematically examine the effects of particle properties and external wall boundary conditions that are not easily controllable in experimental studies. We compare the rising time to a related experimental system [13] and show that the rising of the large particle is very sensitive to wall friction. Furthermore, we show the existence of large-scale force networks when wall friction is present and relate the rise dynamics to formation and destruction of these force networks. We also calculate the force distribution and force correlation within the granular bulk, and discuss their physical implications and similarity to force statistics in granular packs. We propose a graph-theoretic approach based on minimum spanning trees (MST) to analyze the force networks. The multipass MST is shown to capture microstructural information, i.e., the particle configuration and connectivity information, which may be used to define a length scale for continuum modeling. Force statistics are also recovered by the multipass MST algorithm.

In the next section we briefly describe the simulation methodology and computational model setup. In Sec. III, we present results for rising dynamics, force networks and the MST algorithm. In Sec. IV we summarize and conclude this work.

II. MODEL AND METHOD

Molecular dynamics simulations of the Brazil nut problem are performed using a soft sphere model for one large particle and $N-1$ small particles, which interact via contact laws and friction only on contact. Since the realistic modeling of particle deformations is complicated, a simplified contact force and the overlap relation [14], the so-called spring-dashpot model, is used in this work. The principle of the computational model used in the MD simulations is demonstrated in the following.

For two contacting particles $\{i,j\}$, with radii $\{a_i,a_j\}$ at positions $\{\mathbf{r}_i,\mathbf{r}_j\}$, with velocities $\{\mathbf{v}_i,\mathbf{v}_j\}$ and angular velocities $\{\boldsymbol{\omega}_i,\boldsymbol{\omega}_j\}$, (see Fig. 1), the normal compression δ_{ij}, relative normal velocity $\mathbf{v}_{n_{ij}}$, and relative tangential velocity $\mathbf{v}_{t_{ij}}$ are [14]

$$\delta_{ij} = d - r_{ij}, \tag{1}$$

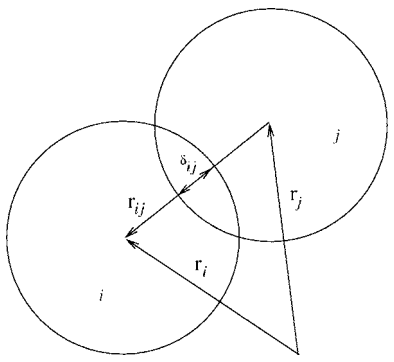

FIG. 1. Schematic of two particles i and j in contact and position vectors $\mathbf{r}_i$, $\mathbf{r}_j$, respectively, with overlap δ_{ij}.

$$\mathbf{v}_{n_{ij}} = (\mathbf{v}_{ij} \cdot \mathbf{n}_{ij})\mathbf{n}_{ij}, \tag{2}$$

$$\mathbf{v}_{t_{ij}} = \mathbf{v}_{ij} - \mathbf{v}_{n_{ij}} - (a_i\boldsymbol{\omega}_i + a_j\boldsymbol{\omega}_j) \times \mathbf{n}_{ij}, \tag{3}$$

where $d=a_i+a_j$, $\mathbf{r}_{ij}=\mathbf{r}_i-\mathbf{r}_j$, $\mathbf{n}_{ij}=\mathbf{r}_{ij}/r_{ij}$, with $r_{ij}=|\mathbf{r}_{ij}|$ and $\mathbf{v}_{ij}=\mathbf{v}_i-\mathbf{v}_j$. The rate of change of the elastic tangential displacement $\mathbf{u}_{t_{ij}}$, set to zero at the initiation of a contact is

$$\frac{d\mathbf{u}_{t_{ij}}}{dt} = \mathbf{v}_{t_{ij}} - \frac{(\mathbf{u}_{t_{ij}} \cdot \mathbf{v}_{ij})\mathbf{r}_{ij}}{r_{ij}^2}. \tag{4}$$

The last term in Eq. (4) arises from the rigid body rotation around the contact point and ensures that $\mathbf{u}_{t_{ij}}$ always lies in the local tangent plane of contact. Normal and tangential forces acting on particle i are

$$\mathbf{F}_{n_{ij}} = f(\delta_{ij}/d)(k_n\delta_{ij}\mathbf{n}_{ij} - \gamma_n m_{\text{eff}}\mathbf{v}_{n_{ij}}), \tag{5}$$

$$\mathbf{F}_{t_{ij}} = f(\delta_{ij}/d)(-k_t\mathbf{u}_{t_{ij}} - \gamma_t m_{\text{eff}}\mathbf{v}_{t_{ij}}), \tag{6}$$

where $k_{n,t}$ and $\gamma_{n,t}$ are the spring stiffness and viscoelastic constants, respectively, and $m_{\text{eff}}=m_im_j/(m_i+m_j)$ is the effective mass of spheres with masses m_i and m_j. The corresponding contact force on particle j is simply given by Newton's third law, i.e., $\mathbf{F}_{ji}=-\mathbf{F}_{ij}$. The function $f(\delta_{ij}/d)=1$ is for the linear spring-dashpot model, and $f(\delta_{ij}/d)=\sqrt{\delta_{ij}/d}$ is for Hertzian contacts with viscoelastic damping between spheres.

Static friction is implemented by keeping track of the elastic shear displacement throughout the lifetime of a contact. The static yield criterion, characterized by a local particle friction coefficient μ, is modeled by truncating the magnitude of $\mathbf{u}_{t_{ij}}$ as necessary to satisfy $|\mathbf{F}_{t_{ij}}| < |\mu\mathbf{F}_{n_{ij}}|$. Thus the contact surfaces are treated as "sticking" when $|\mathbf{F}_{t_{ij}}| < |\mu\mathbf{F}_{n_{ij}}|$, and as "slipping" when the yield criterion is satisfied.

In a gravitational field $\mathbf{g}$, the translational and rotational accelerations of particles are determined by Newton's second law in terms of the total forces acting on each particle i:

$$\mathbf{F}_i^{\text{tot}} = m_i\mathbf{g} + \sum_j \mathbf{F}_{n_{ij}} + \mathbf{F}_{t_{ij}} - b\mathbf{v}_i, \tag{7}$$

and total torques acting on each particle i:

$$\tau_i^{\text{tot}} = -\sum_j a_i\mathbf{n}_{ij} \times \mathbf{F}_{t_{ij}}. \tag{8}$$

The last term $-b\mathbf{v}_i$ in the force equation represents an external damping force. This term is used to artificially enhance the energy dissipation due to two-particle contact, which is underpredicted by the MD contact force model [15,16]. A similar damping term can also arise from the viscous drag a particle experiences due to the presence of an interstitial fluid, but that term is proportional to the relative velocity between particle and fluid.

The amount of energy lost in collisions is characterized by the inelasticity through the value of the coefficient of restitution e, which is defined as the negative ratio of the particle normal velocity after collision to the velocity before collision. For the linear spring-dashpot model, the coefficient of normal restitution and contact time can be analytically obtained:

$$e_n = \exp(-\gamma_n t_c/2), \tag{9}$$

where the contact time t_c is given by

$$t_c = \pi(k_n/m_{\text{eff}} - \gamma_n^2/4)^{-1/2}. \tag{10}$$

The value of the spring constant should be large enough to avoid particle interpenetration, yet not so large as to require an unreasonably small simulation time step δt, since an accurate simulation typically requires $\delta t \sim t_c/50$. After the contact force is calculated, the equations of motion, which are ordinary differential equations, can be numerically integrated to get the particle trajectories.

The computational setup models the experiment in Ref. [13]. In the experimental work, a steel bead was placed at the bottom of a bed of cabbage seeds in a column vibrated by a sinusoidal excitation. The available experimental parameters include the granular bed height of 12 cm; small particle diameter of 0.2 cm, large particle diameter of 0.632 cm, and their densities of 7.8 and 1.1 g/cm^3, respectively; and the sinusoidal vibration with frequency 7.5 Hz and amplitude 1.5 cm. The basic computational parameters are chosen to mimic the experiment as closely as possible, and are listed in Table I. In this computational study, a nondimensional system of equations are solved, where the scaling factors for distance, time, velocity, force, elastic constants, and stresses are d_0, $t_0=\sqrt{d_0/g}$, $v_0=\sqrt{gd_0}$, $F_0=m_0g$, $k_0=m_0g/d_0$, and $\sigma=m_0g/d_0^2$, respectively. The diameter and mass of the small particles are d_0 and m_0.

All the cases were simulated in three dimensions using a molecular dynamics code for granular materials GRANFLOW [14]. The granular media is confined in a cylindrical container, as shown in Fig. 2. The cylinder has a diameter of $12.25d_0$ and the cylinder height is effectively infinite to allow for unrestricted particle rise. The initial particle configuration (Fig. 2) for the large particle is at the bottom of the bed, surrounded by small particles. The initial condition for the segregation simulations is constructed in two steps. First, the large particle is fixed at the bottom and surrounded by small particles. The entire column is vibrated at a high frequency until an equilibrium height is reached; then the frequency is terminated to allow the particles to relax to a ground state, where the total particle kinetic energy is zero. At this state, the particles are arranged in a compact configuration, which is then used as the initial condition for the segregation study. For the case with 6001 particles, the initial bed height is about $43d_0$ and with 7601 particles, the initial height is about $55d_0$. The different heights of the granular pack will be indicated for the cases in the next section. It should be noted that the MD model allows for contact force and friction between the particles and the cylindrical walls in the same way as described for two particles but with infinite mass and diameter for the walls.

In this paper we focus on analyzing segregation using the particle size, mass ratio, and external excitation conditions as specified in Table I. Unlike most experimental work, where these parameters are varied to determine their effect on the

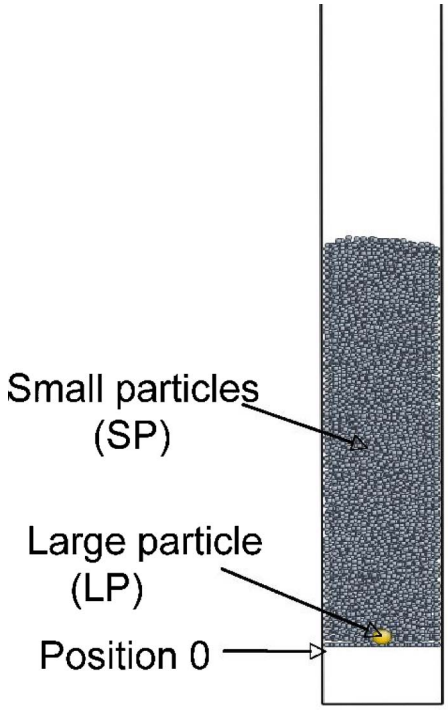

FIG. 2. (Color online) The initial particle configuration as seen in a vertical cut plane through the 3D simulation, with the large particle (in yellow) at the bottom and the surrounding small particles (in grey).

segregation mechanism, we use these parameters as given conditions and investigate other effects that cannot easily be studied by experimental techniques. The effect of wall friction on the Brazil nut rising dynamics as well as the parametric studies are investigated in the next section.

III. RESULTS

A. Brazil nut rising dynamics

The rise time of the large particle is an important phenomenological indicator of segregation in the Brazil nut problem. Although many particle properties needed for the MD simulations are not known from the experiment, a set of computational parameters is established (see Table I) to predict the correct rising behavior of the large particle, i.e., rising from the bottom to the top and fluctuating about an equilibrium height with small amplitudes [17]. The rise time predicted from one simulation is compared with the experimental results [13] as shown in Fig. 3. Note that in this simulation the background damping coefficient $b=0.24$ in $m_0\sqrt{g/d_0}$ units was chosen to obtain a quantitative match with the experimental result, but it is set to zero in the other simulations because it has no effect on the qualitative behavior of the simulated system. Therefore, for all the other simulations the background damping is set to zero, unless otherwise noted.

We perform parametric studies of the BNP to elucidate the effect of MD simulation parameters on rising behavior. We show that this rising behavior is robustly independent of many particle properties but sensitive to wall friction. We first investigate the effect of varying spring stiffness constant. The value of spring stiffness constant $k_n=2\times10^5k_0$ is smaller than the common value of $O(10^{10}k_0)$, which "softens" the particles used in the simulation. However, it is shown in Fig. 4(a) that with increasing spring stiffness, the large particle rise time approaches an asymptotic value, with $k_n=2\times10^5k_0$ giving a rise time close to the asymptotic value. Two different particle contact force models, namely, the linear spring-dashpot model and the Hertzian model, did not change the rising behavior qualitatively, as shown in Fig. 4(b). With the Hertzian model, the large particle rise time was slightly slower and fluctuations in the particle position were reduced.

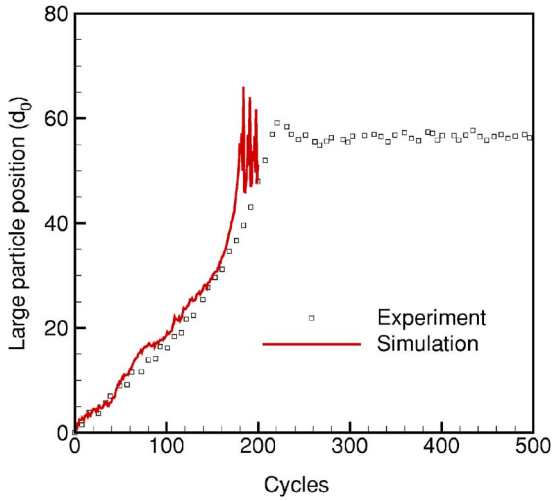

FIG. 3. (Color online) The large particle position as a function of shaking cycles predicted from one simulation case of a granular pack with initial height of $55d_0$ with background damping, $b=0.24$ in $m_0\sqrt{g/d_0}$ units (solid line), compared with the corresponding experimental results (open squires) [13].

Interstitial gas within the granular media may play an important role in the segregation when granular particle sizes are small [11,12]. The interstitial gas flow effect was investigated by modeling air as an incompressible fluid and treating the granular bed as a porous medium, which gives rise to a damping term proportional to the particle slip velocity in the particle force [18]. This damping term is of the same form as the last term in Eq. (7) except that the velocity is the particle *slip* velocity (in place of the particle velocity), and the damping coefficient b is in the range $10^{-3}\sim10^{-2}$ (in $m_0\sqrt{g/d_0}$ units). Comparing the large particle rise time with and without interstitial air effects, it can be seen from Fig. 5(a) that the interstitial air has minimal influence on the rise time. Thus, for this particular problem, the segregation of small and large particles is not adversely affected by the presence of interstitial air, i.e., this is not air-driven segregation.

The effects of small particle polydispersity was examined for a monodispersed case and polydispersed case, where the small particle diameters ranged from $0.9d_0$ to $1.1d_0$. The polydispersed case in Fig. 5(b) demonstrates almost identical rising behavior. Particle friction is another important particle property. Its effects on granular packings has been systematically studied [19,20]. However, its effects on the dynamics in granular systems are still not clear. In this Brazil nut prob-

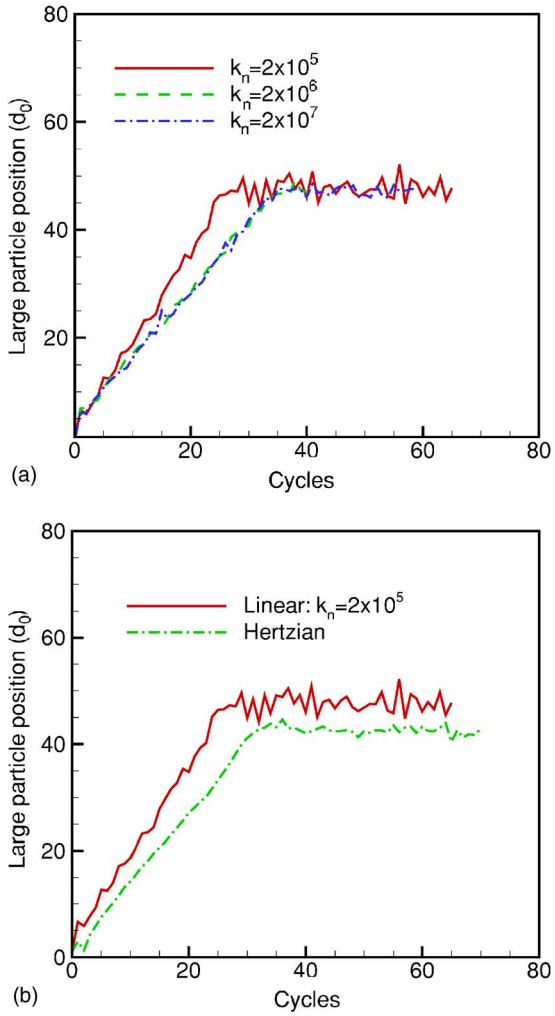

FIG. 4. (Color online) The large particle position as a function of shaking cycles for (a) different values of spring stiffness coefficient k_n and (b) the linear and Hertzian spring-dashpot force models in a granular pack with initial height of $43d_0$.

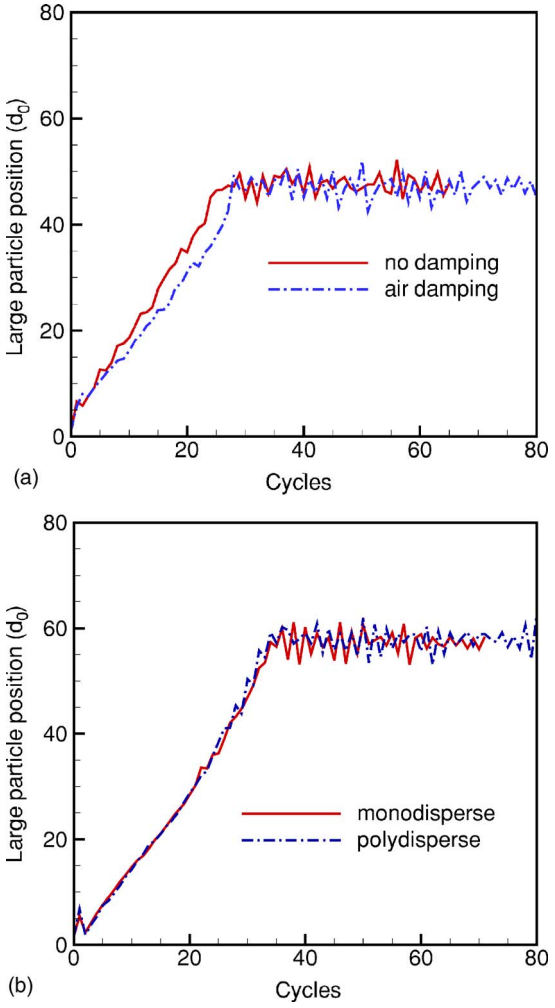

FIG. 5. (Color online) The large particle position as a function of shaking cycles for (a) varying interstitial air damping in a granular pack with initial height of $43d_0$ and (b) small particle size distributions in a granular pack with initial height of $55d_0$.

lem, it is shown that the variation of particle friction coefficient within a reasonable range does not change the rising behavior significantly [Fig. 6(a)]. Even when there is no friction between the particles [Fig. 6(b)], the large particle can still rise when the particle elastic coefficient is set to $k_n=2\times10^6\ k_0$. This excludes particle friction as a necessary condition for the large particle to rise.

However, friction between particles and the confining cylindrical wall, referred to as wall friction hereafter, critically impacts the dynamic response of the granular system. The impact is analogous to the wall friction effects on the internal stress distribution in static granular packings as previously studied by simulations [21] and experiments [22]. The rising behavior of the large particle is very sensitive to wall friction. The large particle oscillates with the granular bed but cannot sustain a rising motion when the wall friction coefficient μ_{wall} is reduced from 0.5 to 0.1 as shown in Fig. 7(a). As μ_{wall} is reduced to zero, the fluctuation in the large particle position becomes larger as shown in Fig. 7(b). Increasing particle stiffness for this situation only decreases the magnitude of the fluctuation and the large particle does not rise. Thus, wall friction is necessary for the large particle to rise.

A comparison between the large particle rising behaviors with ($\mu_{\text{wall}}=0.5$) and without wall friction ($\mu_{\text{wall}}=0.0$), as shown in Fig. 8(a), demonstrates that the large particle rises to the top after 30 cycles and stays at the surface of the granular bed with wall friction. However, without wall friction the large particle oscillates with no regular pattern. A closer look at the displacements for a smaller range of cycles with wall friction, shown in Fig. 8(b), reveals that the center of mass of the small particles and the large particle, vary in a one-cycle pattern. It is, therefore, worthwhile to analyze the dynamics of particles within one cycle. Taking a window from cycle 10 to cycle 11, as shown in Fig. 9, it can be observed from both the displacements [Fig. 9(a)] and the velocities [Fig. 9(b)] that the entire granular bed loses contact with the vibrating base at approximately $T=10.05$ when the acceleration equals $-g$, and subsequently impacts with the base at around $T=10.85$. The stage from $T=10.05$ to 10.85 is defined as the expansion stage since the granular bed experiences dilatation during this period, while the rest of the

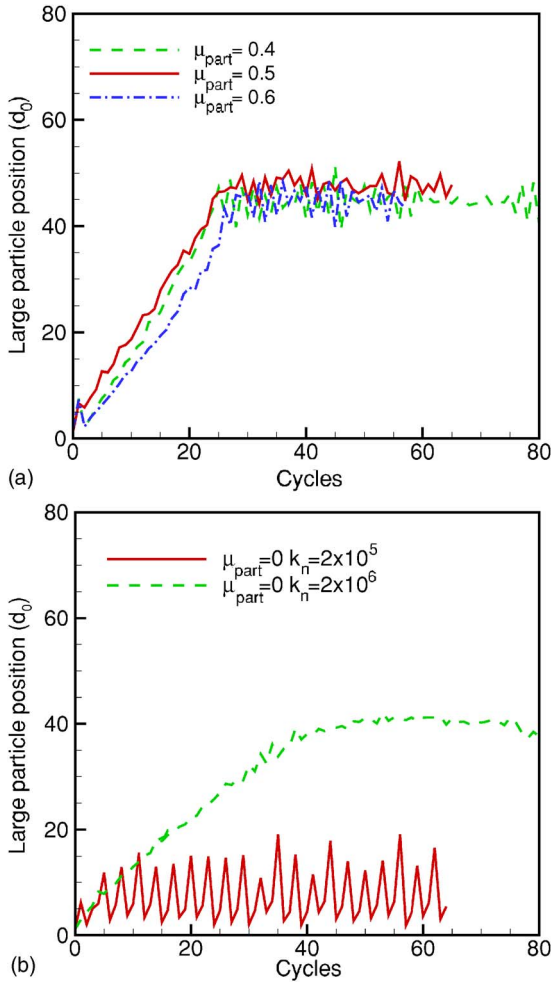

FIG. 6. (Color online) The large particle position as a function of shaking cycles for (a) different particle friction coefficients and (b) different spring stiffness constants in a granular pack with initial height of $43d_0$.

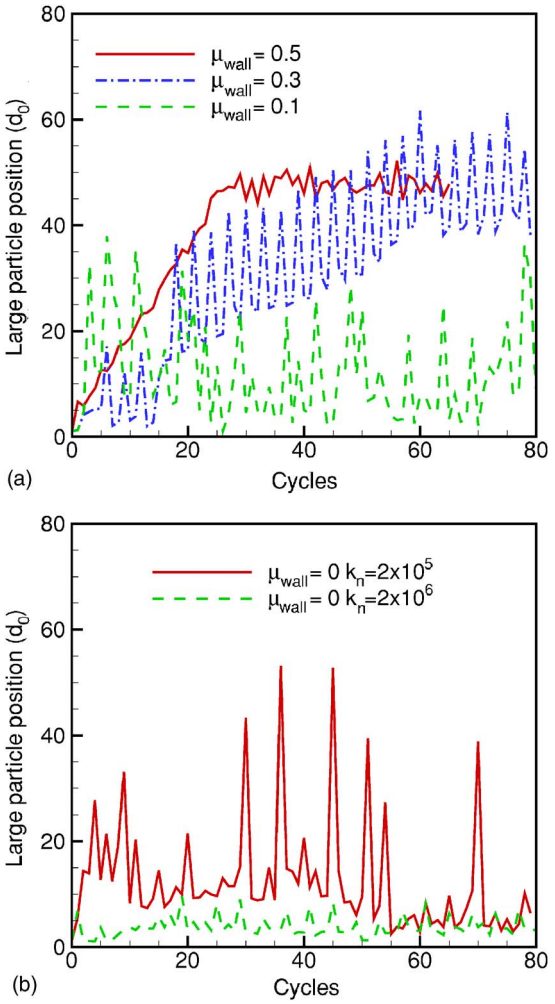

FIG. 7. (Color online) The large particle position as a function of shaking cycles for (a) different wall friction coefficients and (b) different spring stiffness constants for no wall friction in a granular pack with initial height of $43d_0$.

cycle is defined as the compression stage corresponding to compaction of the granulates. These concepts will be further elucidated by the microstructural analysis presented in the next section.

In the expansion stage, the large particle experiences a free rise and fall together with the small particles [the height gained by the large particle can be obtained from the displacement data in Fig. 9(a), and it is close to $\sqrt{v^2/2g}$ calculated from the velocity data from Fig. 9(b)]. However, in the compression stage, the large particle quickly adjusts to the vibration velocity which is transmitted through a strong force network. The large particle's velocity is greater than the velocity of the center mass of small particles [Fig. 9(b)]. As a result the large particle rises to a higher position at cycle 11 than that at the beginning of cycle 10 [Fig. 9(a)]. The reason behind this dynamical variation is closely related to the force network formation and destruction in one cycle as demonstrated in the next section.

B. Force networks and statistics

It is natural to speculate whether there exist structures in nonfluidized granular media [13], similar to the force networks in static packings [20] or arches shown in two-dimensional vibrating piles [9,23]. This is indeed the case as shown in the following data analysis, where the interaction between structures and dynamics is revealed.

Average coordination number, defined as the average number of contacts per particle, is a measure that is sensitive to the local particle configuration and has been used to characterize the static mechanical equilibrium state in static packing [19]. In the dynamic problem studied in this paper, the time evolution of the coordination number averaged over all the particles in granular media is used to understand the dynamic response of the system and the corresponding structural information at each instance. As shown in Fig. 10(a), the average coordination number for the granular system with wall friction $\mu_{\text{wall}}=0.5$ shows a periodic pattern, while the one for the granular system without wall friction shows an irregular pattern. It can be seen from the evolution of the average coordination number within one cycle in Fig. 10(b), that the average coordination number falls below unity during the expansion stage, indicating most particles have no contact. However, the average coordination number in the

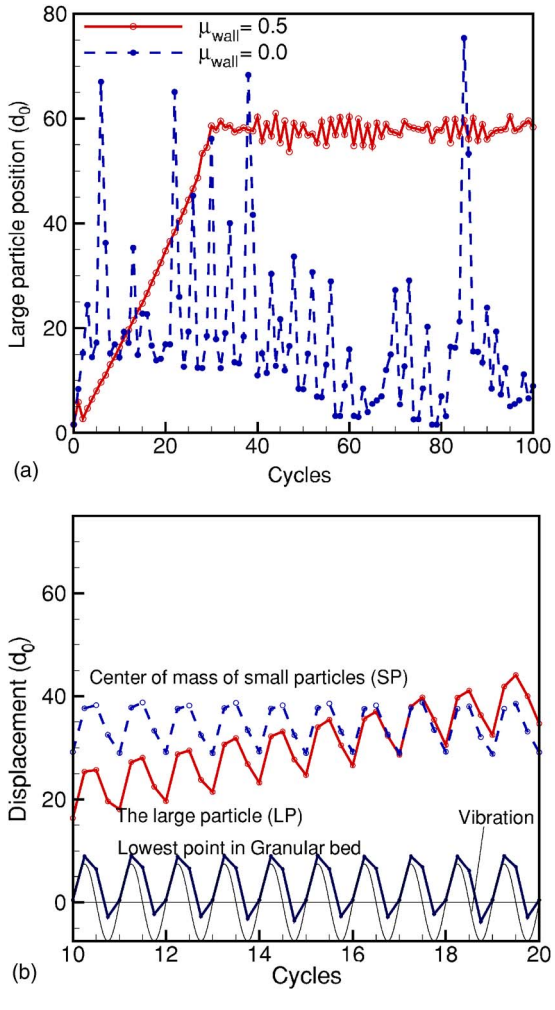

FIG. 8. (Color online) The large particle position as a function of the shaking cycles for (a) varying wall friction μ_{wall} and (b) particle positions for the case with wall friction ($\mu_{\text{wall}}=0.5$) from $T=10$ to $T=20$ in a granular pack with initial height of $55d_0$. The sinusoidal curve is shown to illustrate the vibration frequency.

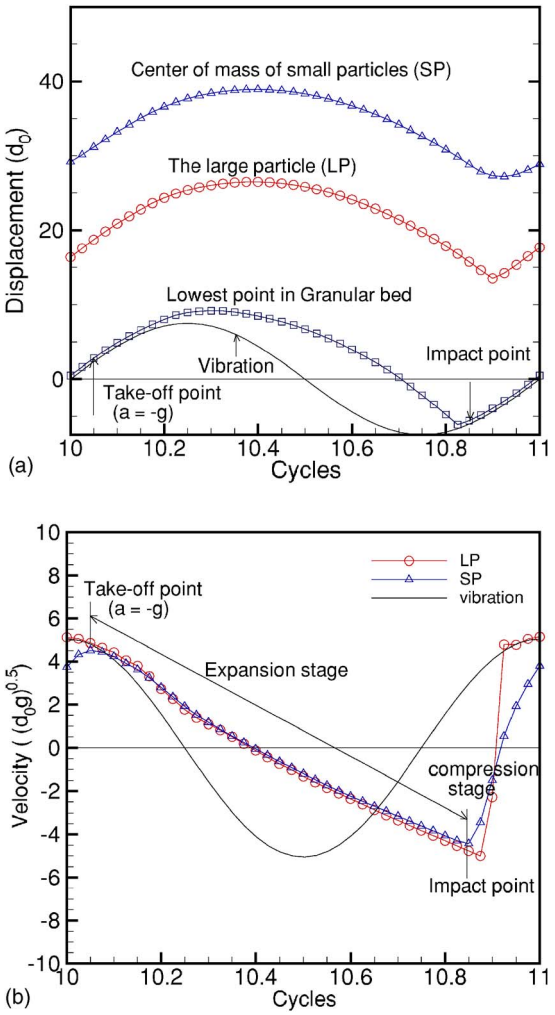

FIG. 9. (Color online) Changes in (a) particle displacements and (b) velocities within one cycle for the case with wall friction in a granular pack with initial height of $55d_0$. The sinusoidal curve is shown to illustrate the vibration frequency.

compression stage rises to 3, indicating there are multiple contacts for a particle and suggesting the presence of a force network during this stage.

To provide direct evidence of the existence of force networks during the compression stage, a graph algorithm was used to identify force networks. A force network is defined as a collection of particles such that every particle in the force network is in contact with at least one other particle, and each particle has a nonzero normal contact force. For the case with wall friction and a total of 7601 particles, the total number of force networks at $T=10$ is 80. These networks range from the minimum of two particles in contact to a very large network with many particles. It is found that at the time instant when the average coordination number reaches it maximum value of 3.2, most particles are indeed in a large force network. Of the total number of 7601 particles, 5796 particles (including the large particle) are in a force network with a network-averaged coordination number of 3.98.

Therefore, the lack of a strong force network during expansion stage allows the large particle move freely. The force network in the compression stage, however, supports the large particle and transmits the velocity boundary condition directly to the large particle. Since not all the small particles are in the same force network, their average velocity is not the same as that of the large particle.

A corresponding force network analysis for the case with $\mu_{\text{wall}}=0$ reveals that there are no large force networks for most of the cycle, and the magnitude of the forces is much smaller than that with wall friction present. Configurations of the force network are visualized comparing the cases with and without wall friction in Figs. 11(a) and 11(b), respectively. In both figures, for clarity only connections between particles whose normal contact force F_n is greater than the average normal contact force $\bar{F}_n$ are shown. From Fig. 11(a), it can be clearly seen that extended force-bearing structures exist over a long length scale with wall friction; in contrast, there are no large force networks with strong forces when there is no wall friction, which results in the oscillation of the large particle.

Further analysis of the largest force network with 5796 particles reveals a strong subnetwork of 3375 particles, which carries forces $F_n > \bar{F}_n$, where $\bar{F}_n$ is the average normal

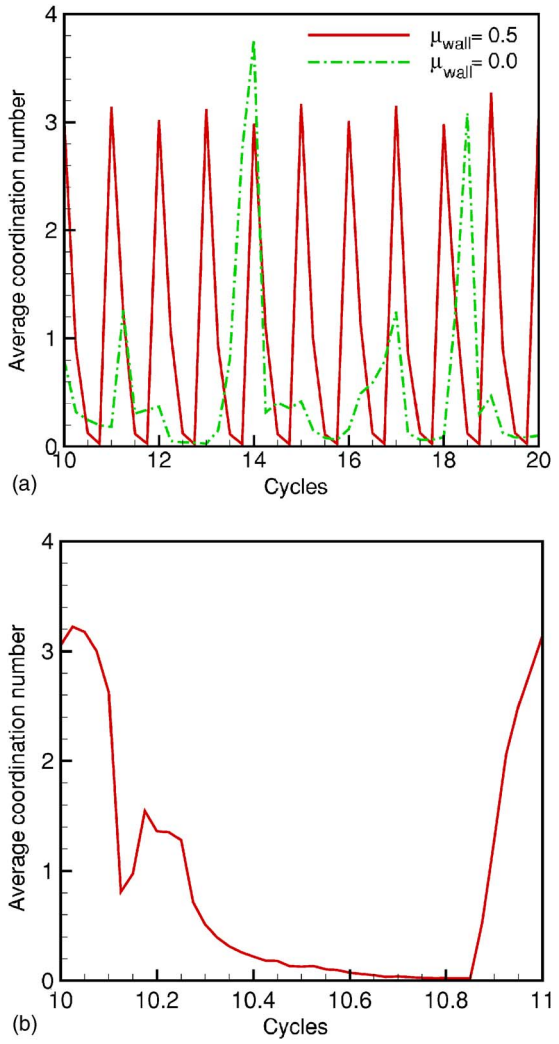

FIG. 10. (Color online) Time evolution of the average coordination number for all the particles (a) varying within 10 cycles and (b) varying within one cycle for $\mu_{\text{wall}}=0.5$ in a granular pack with initial height of $55d_0$.

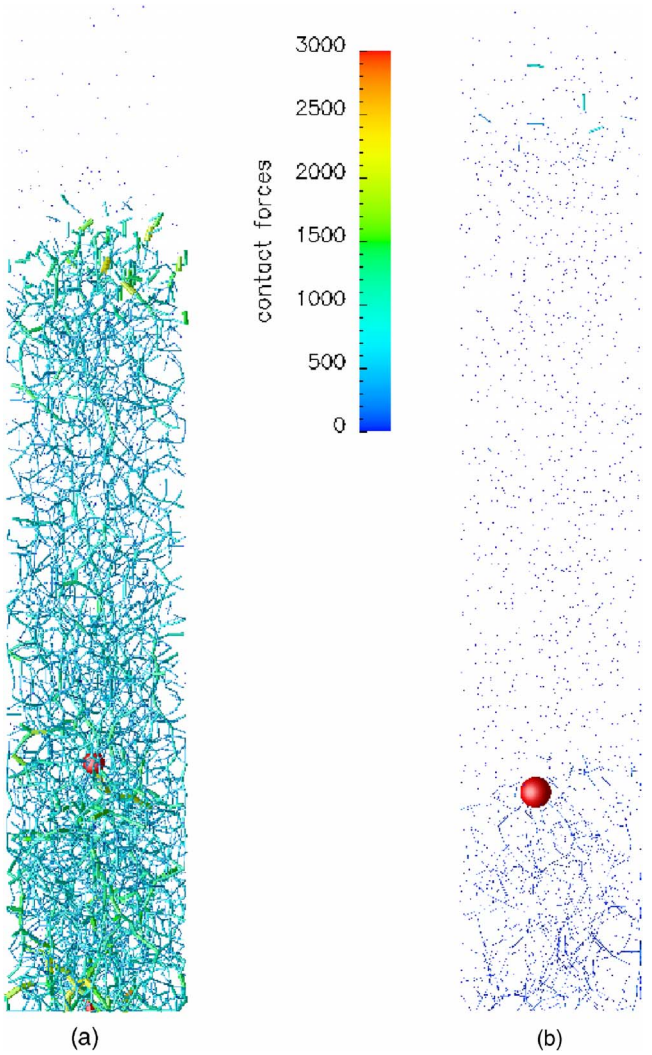

FIG. 11. (Color online) Force networks in the granular media at cycle 10 for (a) $\mu_{\text{wall}}=0.5$ and (b) $\mu_{\text{wall}}=0.0$. In the figures, both the edge thickness and color scales are proportional to the magnitude of normal forces. The (red) sphere indicates the position of the large particle and the dots indicate the positions of small particles. Only the edge with forces $F_n > \bar{F}_n$ are shown.

contact force. This indicates a wide distribution of forces in the force networks. The statistics of all normal forces in the force networks are characterized by the probability density function (PDF) of the scaled forces $f=F_n/\bar{F}_n$. The PDF at $T=10$ for $\mu_{\text{wall}}=0.5$ is shown in Fig. 12(a). The PDF shows the generic feature of the force distribution in static granular packings [20,24], i.e., it exhibits a peak (plateau) for small forces ($f<1$) and exponential decay for large forces ($f>1$). Mueth *et al.* [24] fitted their experimental data with an empirical function of the form

$$P(f) = a(1 - be^{-f^2})e^{-\beta f}, \tag{11}$$

and found $a=3.0$, $b=0.75$, and $\beta=1.5\pm0.1$ for a static packing of glass spheres in a cylindrical container. To compare with the static packing experimental data, we fit Eq. (11) to our computational data and find the function with $a=2.46$, $b=0.83$, and $\beta=1.35$ agrees well with the force distribution in the force networks as shown in Fig. 12(a). For the expansion stages and the case where $\mu_{\text{wall}}=0.0$, the number of contact forces is small and the PDF of forces suffers from large statistical error due to insufficient samples. Therefore, the PDF for those situations is not discussed here.

In addition to the PDF of the force distribution, the force pair correlation was also computed with the aim of characterizing the force correlation length. The spatial force-force correlation function $\mathcal{F}(r)$ measures spatial correlations between forces separated by a distance r. We use the same definition as in Refs. [20,24]:

$$\mathcal{F}(r) \equiv \frac{\sum_i \sum_{j>i} \delta(r_{ij} - r) f_i f_j}{\sum_i \sum_{j>i} \delta(r_{ij} - r)}, \tag{12}$$

where r_{ij} is the distance between particle contacts i and j, and f_i is the normalized contact force acting at contact i.

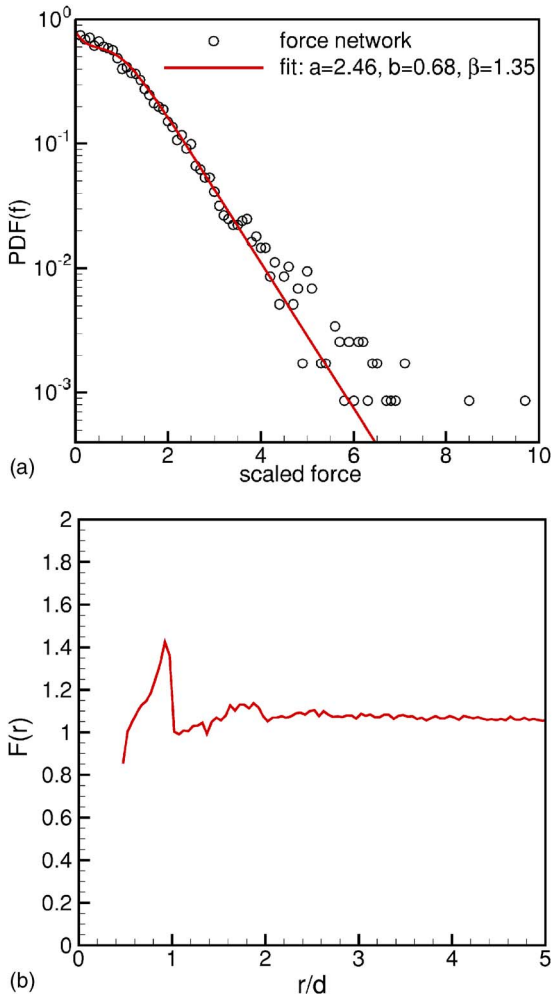

FIG. 12. (Color online) (a) Probability densities for normal contact force based on all contacts from the computed data (open circles) and fitted with Eq. (11) (solid line) using $a=2.46$, $b=0.68$, and $\beta=1.35$. (b) Force correlation function constructed from all contact forces.

Note that this isotropic expression for the radial spatial force correlation formulation is not strictly applicable to the anisotropic system of finite size that is considered in this paper. However, the result for r smaller than the radius of the granular column still gives some insight to the force correlations. The result at $T=10$ for $\mu_{\text{wall}}=0.5$ produces peaks around $r=d_0$ and dies out after $3d_0$ as shown in Fig. 12(b), indicating a diffusive nature of the force transmission network. This behavior is again similar to the force correlation in a granular packing [20]. It is interesting to note that the force correlation length scale is much smaller than the geometric contact length scale of $52.2d_0$.

C. Minimum spanning tree

As shown in Sec. III B, there are force networks and structures existing in this Brazil nut problem. It is difficult to directly represent this structural information in a continuum model for the stress tensor. We explore the possibility of using a numerical algorithm based on particle position information to capture the microstructures and provide structural information in a statistical sense, i.e., we seek to determine if a representative subensemble of the particles can capture the important statistics of the force network and if there is a convergent procedure to determine this representative subensemble. We show that a modified minimum spanning tree (MST) approach is indeed capable of achieving this goal.

Constructing an Euclidean MST (EMST) on N particles requires connecting every particle with at least one neighbor particle through an edge (an unordered pair of particles). Since every particle is connected in the EMST it possesses the spanning property. A tree is a set of edges that contains no closed loops or cycles; i.e., starting from a particle and tracing an alternating sequence of edges between particles does not lead back to the initial particle. Finally, since it is a Euclidean minimum spanning tree, the sum of the Euclidean lengths of these edges is a minimum. A formal graph-theoretic definition of a minimum spanning tree (MST) and algorithms for constructing an MST can be found in the literature [25,26]. The minimum spanning tree has been previously employed in a mixing model for turbulent reactive flows, where it was constructed on an ensemble of particles in composition space to provide a definition of localness [27].

An example of constructing the MST based on particle positions is illustrated in Fig. 13, where particles 1, 2, and 3 are all in contact with each other, while particles 4 and 5 are in contact with each other but not with the others. Let the length of the edges be the distance between the centers of two particles in Euclidean space. If the length $E(1,3)$ of the edge between particle 1 and particle 3 is greater than $E(1,2)$ or $E(2,3)$ due to difference in normal compression at contact, then the resulting MST is shown in Fig. 13(a) by the lines connecting the centers of particles. If the lengths of $E(1,2)$, $E(1,3)$, and $E(2,3)$ equal each other, then any two of the these three edges can be selected in the MST, which in this case is nonunique.

Not all the edges in the MST correspond to the force network. Since particles 3 and 4 are not in contact, $E(3,4)$ does not contribute to the normal contact force statistics and is deleted when studying the force statistics produced from the MST. As shown in Fig. 13(b), deleting $E(3,4)$ from the MST results in two subtrees of contacting particles. A tree of contacting particles (TCP) is defined by the number of contacting particles N_P and the set of N_E edges that define the contacts between the particles. Therefore, the TCPs contain important particle configuration information: how many particles N_P are in a force network, and which particles are connected (from the set of edges). From the MST we recover information relevant to the force networks by deleting noncontacting edges and identifying the resulting TCPs as the force networks.

As the first step toward applying the MST, we will show that the MST constructed on the particle positions can capture the majority of structural information pertaining to force networks within granular media. Then using a multipass MST technique, we show that almost all the contacts can be recovered from MST in just a few passes, and so can the force statistics.

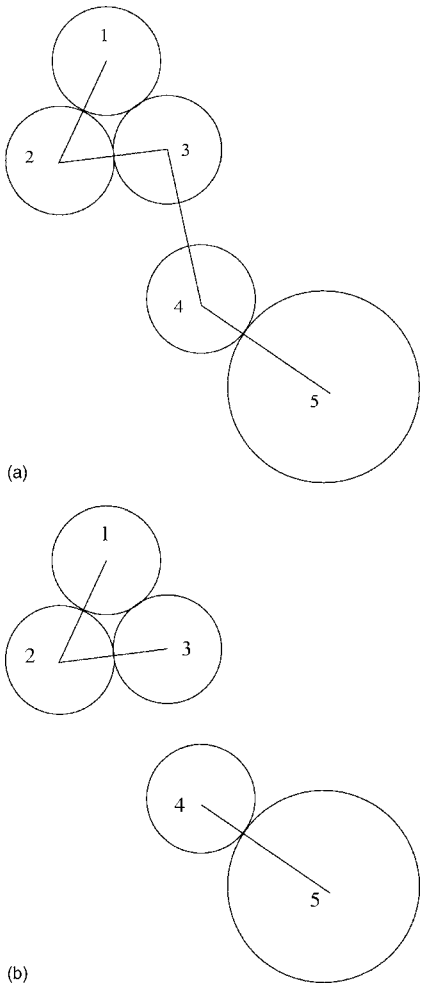

FIG. 13. Schematics of the MST constructed based on (a) particle positions and (b) the subtrees after deleting edges between noncontacting particles. The particles are represented by circles and the edges are shown by the lines connecting centers of particles.

Due to the minimum spanning property of a MST, at least one contact for a particle can be captured in the MST if there exist contacts for that particle in monodispersed particle configurations. If the MST is formed on all the particles and the noncontacting edges are deleted to form the TCP's, it is shown in the row corresponding to the first pass of Table II that the number of particles, N_P in the largest TCP and number of other TCPs, N_T, are exactly the same as those from the MD force network. The distribution of TCPs with respect to the number of particles in a TCP can also be shown to be exactly the same as that obtained from the MD force networks. The MST can thus predict the geometric length scale present in a force network, such as the maximum distance between two particles in a TCP or a force network. This length scale is $52.2d_0$ for the largest TCP or the largest force network. However, the MST does not capture all the particle contacts in the TCPs. Since there is no closed loop in a MST, some edges forming a closed loop in a force network are neglected. Since the MST cannot capture multiple contacts in a single pass [see Fig. 13(b) where only two of the three contacting edges for particle 1, 2, and 3 are selected by the MST algorithm], the number of edges N_E in the first pass of the MST [28] is only 5795, as compared to the 11 533 edges in the MD force network (see Table II).

TABLE II. Number of edges and TCPs captured by MST and comparison with all force networks from MD.

	The largest TCP		The rest of TCPs	
Passes	N_P	N_E	N_T	N_E
1	5796	5795	79	106
2	5796	10505	79	106
3	5796	11508	79	106
4	5796	11515	79	106
5	5796	11516	79	106
Force networks	5796	11533	79	106

To capture all the edges in a force network, a multipass MST technique is proposed. A second pass of MST is constructed by preferentially weighting edges that have already been selected in previous passes of MST. The lengths of the edges selected in previous passes are elongated by a specified factor in this case. Referring to the example shown in Fig. 13, the edge $E(1,3)$ is not selected in the first pass. A second pass of MST is constructed on the same particles after elongating the lengths of previously selected edges $E(1,2)$, $E(2,3)$, and $E(4,5)$ by a factor of 1.2. In this way, the edge $E(1,3)$ will be selected in the second pass of the MST. As shown in Table II, the one-pass MST captured 5795 edges for the largest MST and 106 edges for the other TCPs, although there are a total of 11533 edges in the largest force network. The two-pass MST captured more than 90% of total edges (repeated edges are not counted). The number of edges N_E in the largest TCP captured by the multipass MST increases with increasing number of passes, as shown in Table II and rapidly converges to the total number of edges in the MD force network. In fact, all the edges have been recovered by a four-pass MST except 18 edges connecting the large particle, which are much longer than other edges and difficult to capture using the current multipass MST algorithm. Note that the number of particles in the largest TCP stays the same since this information is faithfully captured by the one-pass MST as discussed before.

Assigning the forces from the force networks to the corresponding edges in the MST, we can determine how well the MST captures force statistics. The force PDF obtained from the MST is compared with that obtained from the force networks in Fig. 14. It can be seen that most of the forces in the one-pass MST are larger than the mean force due to the minimum spanning property. This is indicated by higher probabilities for the larger force and lower probabilities for the smaller-than-mean forces. The one-pass MST also preserves the exponential decay for larger force values. The force distributions generated by various passes of MST are also fitted to quantitatively demonstrate these statistical characteristics. We find that the PDF can be fitted with a functional form

$$P(f) = a(1 - be^{-(f-\alpha)^2})e^{-\beta(f-\gamma)}. \tag{13}$$

We fit the forces captured by the one-pass MST using $\alpha = \gamma = 0.45$ and the same values of a, b, and β as those used for

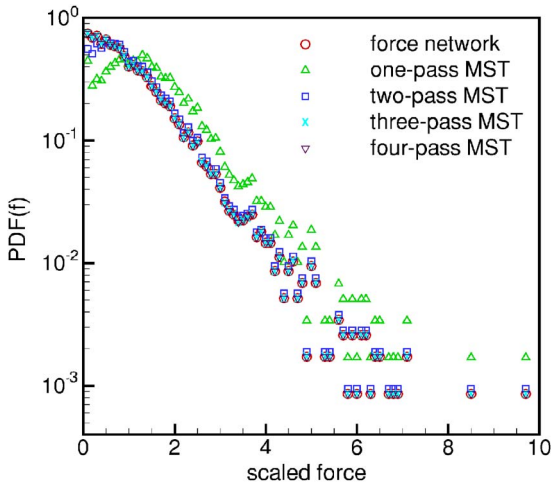

FIG. 14. (Color online) Probability densities for normal contact forces based on all contacts (force networks) and constructed from multipass MST. The PDF of all contact forces is overlapped by the multipass MST results; however, it can also be seen in Fig. 12(a) for clarity.

fitting the forces in the force networks. This fitting indicates that the force PDF for MST is shifted toward larger forces by the magnitudes of α and γ. It is shown in Fig. 15(a) that the exponential decay for the larger forces is fitted well while the smaller forces have smaller probabilities compared with the fitting. This result means that the one-pass MST oversampled larger forces, but with the same decay rate compared to the force distribution in the force networks. Furthermore, we find that Eq. (13) fits the whole range of forces well with $a=2.2$, $b=0.9$, $\beta=1.35$, $\alpha=0.25$, and $\gamma=0.5$, which is demonstrated in the inset of Fig. 15(a). The two-pass, three-pass, and four-pass MST quickly converge to the PDF from the force networks, with almost no distinction between them after three passes. The fit to the two-pass MST force PDF is done using $\alpha=\gamma=0.1$ to shift the fitted force networks PDF and shows good agreement for the larger forces in Fig. 15(b). Similarly, Eq. (13) with $a=3.1$, $b=0.8$, $\beta=1.35$, $\alpha=-0.1$, and $\gamma=-0.1$ fits the whole range of forces well as shown in the inset of Fig. 15(b). For the three-pass and four-pass MST PDF, the fitted force networks PDF also fits well, i.e., $\alpha=\gamma=0$. Overall, α and γ decrease to zero with the increasing of number of MST passes and thus Eq. (13) recovers to Eq. (11), which shows the multipass MST is a convergent procedure to capture forces in the force networks. The same convergence was found for the force correlation functions as shown in Fig. 16. Thus the modified MST algorithm is able to recover particle configuration information as well as statistics and spatial correlation of the normal contact forces.

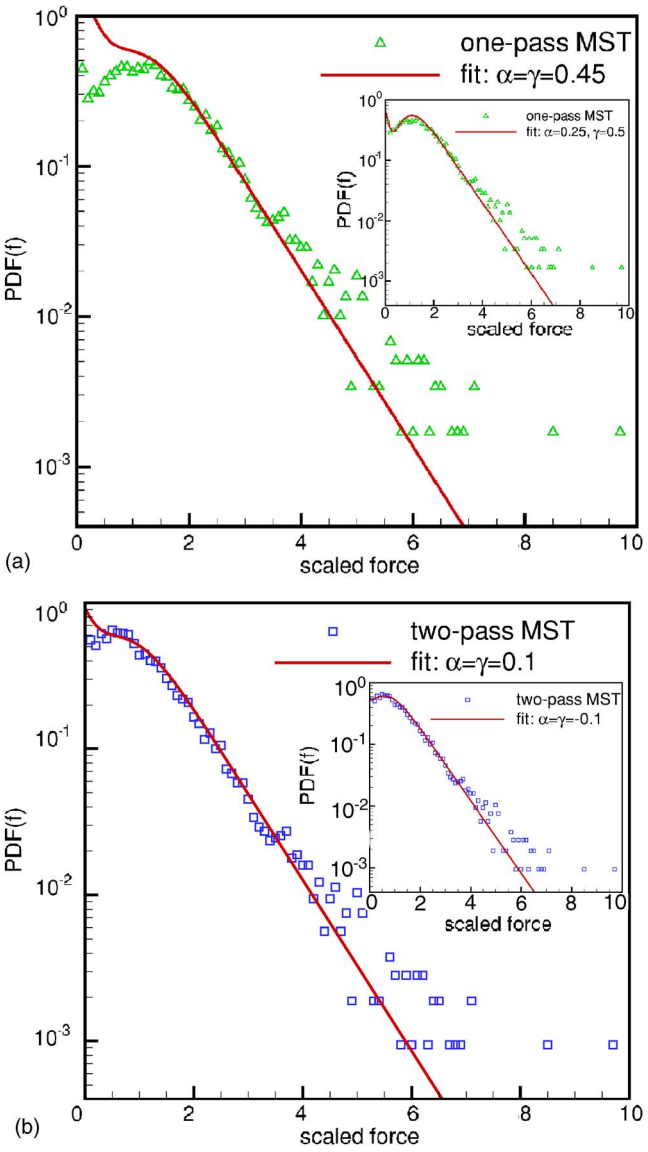

FIG. 15. (Color online) (a) Probability densities for normal contact force based on the contacts from the one-pass MST(open triangles) and fitted with Eq. (13) (solid line) using $a=2.46$, $b=0.83$, $\beta=1.35$, $\alpha=0.45$, and $\gamma=0.45$. Inset: the one-pass MST data is fitted with Eq. (13) (solid line) using $a=2.2$, $b=0.9$, $\beta=1.35$, $\alpha=0.25$, and $\gamma=0.5$. (b) Probability densities for normal contact force based on the contacts from the two-pass MST (open squires) and fitted with Eq. (13) (solid line) using $a=2.46$, $b=0.83$, $\beta=1.35$, $\alpha=0.1$, and $\gamma=0.1$. Inset: the two-pass MST data is fitted with Eq. (13) (solid line) using $a=3.1$, $b=0.8$, $\beta=1.35$, $\alpha=-0.1$, and $\gamma=-0.1$.

IV. CONCLUSIONS

We have performed MD simulations of the BNP at low vibration frequency in order to understand the underlying physical mechanisms of segregation dynamics. Systematic variation of the particle properties and external wall friction reveals that the large particle rising is not sensitive to particle stiffness, interaction force models, interstitial air effects, slight polydispersity in small particles, or particle friction. However, the rise time is very sensitive to external wall friction. We conclude that wall friction is the most important physical parameter in determining the segregation behavior in this BNP. We also show the one-cycle dynamical response of the granular bed with wall friction ($\mu_{\text{wall}}=0.5$), within which there is an expansion stage and a compression stage.

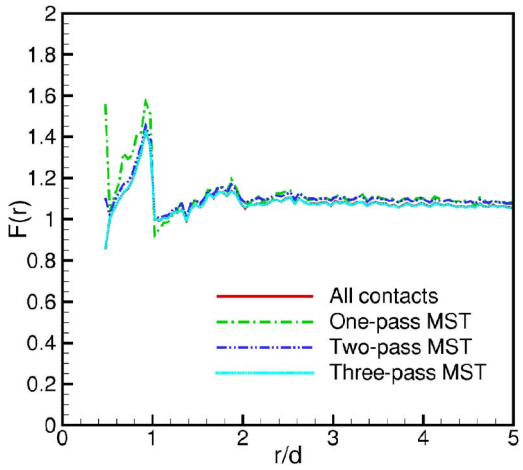

FIG. 16. (Color online) Force correlation function constructed from all contact forces and constructed from multipass MST. The force correlation function of all contact forces is overlapped by the multipass MST results; however, it can also be seen in Fig. 12(b) for clarity.

The granular bed exhibits irregular oscillation without wall friction ($\mu_{\text{wall}}=0.0$).

We found the presence of large-scale force networks bearing larger-than-average forces in the compression stage with wall friction, while there are much fewer contacts in the expansion stage. However, without wall friction such large strong force networks do not exist. We analyzed the force network by comparing the PDF of normal contact forces and found exponential tails similar to those found in packing experiments. We further analyzed the two-point force correlation of the force network and found force correlations decay quickly. The fact that the length scale over which the normal force is correlated is only two to three particle diameters, whereas the geometric contacts extend over $50d_0$ (the size of the system), indicates that a local interaction model for the force on a particle is adequate. However, the large length scale of geometric contact appears to be essential for transmission of the effect of wall friction. Therefore, one can conclude that the geometric length scale indicates the nature of the material response: if it is small, the particle behaves as an isolated free body, if it is large, the granular material behaves like a continuum composed of grain skeletons. Yet, even this continuum can admit a local force or stress model because of the short-range nature of the contact force.

Finally, we applied the Euclidean minimum spanning tree to analyze the force network, and explored the possibility of using MST based on particle position information to capture the microstructures and provide structural information in a statistical sense. We showed that the MST is able to capture the complete structural information. We developed a multipass MST algorithm, which was able to recover all the contacts within the force network and thus was able to recover the force distribution and force correlation for the force network. Therefore, the MST provides a possible route to constructing a continuum model with microstructural information supplied from this algorithm.

ACKNOWLEDGMENTS

This work received partial support through Contract No. W-7405-ENG-82 with the U.S. Department of Energy. J.S. would like to thank Steve Plimpton for his help with GRANFLOW.

[1] The Brazil nut is a name coined from the observed behavior of shaking a can of mixed nuts and noting that the Brazil nut rises to the top.
[2] A. Rosato, K. J. Strandburg, F. Prinz, and R. H. Swendsen, Phys. Rev. Lett. **58**, 1038 (1987).
[3] A. D. Rosato, D. L. Blackmore, N. Zhang, and Y. Lan, Chem. Eng. Sci. **57**, 265 (2002).
[4] D. A. Huerta and J. C. Ruiz-Suárez, Phys. Rev. Lett. **92**, 114301 (2004).
[5] J. B. Knight, H. M. Jaeger, and S. R. Nagel, Phys. Rev. Lett. **70**, 3728 (1993).
[6] D. A. Huerta and J. C. Ruiz-Suárez, Phys. Rev. Lett. **93**, 069901(E) (2004).
[7] N. Shishodia and C. R. Wassgren, Phys. Rev. Lett. **87**, 084302 (2001).
[8] L. Trujillo, M. Alam, and H. Herrmann, Europhys. Lett. **64**, 190 (2003).
[9] J. Duran, J. Rajchenbach, and E. Clément, Phys. Rev. Lett. **70**, 2431 (1993).
[10] M. E. Möbius, B. E. Lauderdale, S. R. Nagel, and H. M. Jaeger, Nature (London) **414**, 270 (2001).
[11] N. Burtally, P. King, and M. Swift, Science **295**, 1877 (2002).
[12] M. E. Möbius, X. Cheng, G. S. Karczmar, S. R. Nagel, and H. M. Jaeger, Phys. Rev. Lett. **93**, 198001 (2004).
[13] Y. Nahmad-Molinari, G. Canul-Chay, and J. C. Ruiz-Suárez, Phys. Rev. E **68**, 041301 (2003).
[14] L. E. Silbert, D. Ertas, G. S. Grest, T. C. Halsey, D. Levine, and S. J. Plimpton, Phys. Rev. E **64**, 051302 (2001).
[15] S. Luding, in *The Physics of Granular Media*, edited by H. Hinrichsen and D. E. Wolf (Wiley-VCH Verlag, New York, 2004), p. 299.
[16] S. Luding, E. Clément, A. Blumen, J. Rajchenbach, and J. Duran, Phys. Rev. E **50**, 4113 (1994).
[17] Fluctuations about the equilibrium height occur due to impacts with the top layer particles which are not confined in the upward direction. In this paper, only the simulaitons with small fluctuations are considered, which excludes the reentrance phenomena.
[18] P. Biswas, P. Sanchez, M. R. Swift, and P. J. King, Phys. Rev. E **68**, 050301(R) (2003).
[19] L. E. Silbert, D. Ertas, G. S. Grest, T. C. Halsey, and D. Levine, Phys. Rev. E **65**, 031304 (2002).
[20] L. E. Silbert, G. S. Grest, and J. W. Landry, Phys. Rev. E **66**, 061303 (2002).
[21] J. W. Landry, G. S. Grest, L. E. Silbert, and S. J. Plimpton, Phys. Rev. E **67**, 041303 (2003).

[22] L. Vanel and E. Clément, Eur. Phys. J. B **11**, 525 (1999).
[23] J. Duran, T. Mazozi, E. Clement, and J. Rajchenbach, in *Fractal Aspects of Materials*, edited by F. Family *et al.*, MRS Symp. Proc. No. 367 (Materials Research Society, Pittsburgh, 1995), p. 491.
[24] D. M. Mueth, H. M. Jaeger, and S. R. Nagel, Phys. Rev. E **57**, 3164 (1998).
[25] A. V. Aho, J. E. Hopcroft, and J. D. Ullman, *Data Structures and Algorithms* (Addison-Wesley, Reading, MA, 1983).
[26] F. P. Preparata and M. I. Shamos, *Computational Geometry: An Introduction* (Springer-Verlag, New York, 1985).
[27] S. Subramaniam and S. B. Pope, Combust. Flame **115**, 487 (1998).
[28] An MST on N_P particles will always have N_P-1 edges.